Molecular dynamics simulations of head-on low-velocity collisions between particles

Yuki Yoshida [1,*] Eiichiro Kokubo,[2] and Hidekazu Tanaka[3]

[1]*Center for Planetary Science, Kobe University, 7-1-48 Minatojimaminami, Chuo-ku, Kobe, Hyogo 650-0047, Japan,*
[2]*Center for Computational Astrophysics, National Astronomical Observatory of Japan, 2-21-1 Osawa, Mitaka, Tokyo 181-8588, Japan*
[3]*Astronomical Institute, Graduate School of Science, Tohoku University, 6-3 Aramaki, Aoba-ku, Sendai 980-8578, Japan*

The particle contact model is important for powder simulations. Although several contact models have been proposed, their validity has not yet been well established. Therefore, we perform molecular dynamics (MD) simulations to clarify the particle interaction. We simulate head-on collisions of two particles with impact velocities less than a few percent of the sound velocity to investigate the dependence of the interparticle force and the coefficient of restitution on the impact velocity and particle radius. In this study, we treat particles with a radius of 10–100 nm and perform simulations with up to 0.2 billion atoms. We find that the interparticle force exhibits hysteresis between the loading and unloading phases. Larger impact velocities result in strong hysteresis and plastic deformation. For all impact velocities and particle radii, the coefficient of restitution is smaller than that given by the Johnson-Kendall-Robert theory, which is a contact model that gives the force between elastic spherical particles. A contact model of inelastic particles cannot reproduce our MD simulations. In particular, the coefficient of restitution is significantly reduced when the impact velocity exceeds a certain value. This significant energy dissipation cannot be explained even by the contact models including plastic deformation. We also find that the coefficient of restitution increases with increasing particle radius. We also find that the previous contact models including plastic deformation cannot explain the strong energy dissipation obtained in our MD simulations, although they agree with the MD results for very low impact velocities. Accordingly, we have constructed a new dissipative contact model in which the dissipative force increases with the stress generated by collisions. The new stress-dependent model successfully reproduces our MD results over a wider range of impact velocities than the conventional models do. In addition, we proposed another, simpler, dissipative contact model that can also reproduce the MD results.

I. INTRODUCTION

Particle collisions are universal processes that occur in many fields of science and technology (e.g., Refs. [1–3]). In mineral-processing engineering, for example, fine ores form agglomerates such as pellets; particle collision processes are essential for their formation, growth, and fragmentation. In the fertilizer industry, agglomeration technology is used to form granules. In astrophysics, dust aggregates—the starting materials of planets—are formed by many silica and water ice particles. In this process, submicron-sized dust particles stick together at collision velocities of $\lesssim 100$ m/s to form agglomerates. Furthermore, the structure of the small bodies of the solar system is described by the granular mechanic's theories, which have been studied theoretically, experimentally, and numerically (e.g., Ref. [4]).

Powder simulations have been used to study the physics of agglomerates, including the structures and tensile strengths of agglomerates, the threshold collision velocity for fragmentation, and fragment distributions (e.g., Refs. [5–10]). In powder simulations, the interaction forces and torques between particles are usually calculated assuming spherical

particles. Several contact models have been proposed for spherical particles. The Johnson–Kendall–Roberts (JKR) theory [11–15] is the model often used in the powder simulations (e.g., Refs. [5–10]). The JKR theory assumes a pressure distribution in which the pressure diverges at the rim of the contact region. This model is consistent with the experiments that use large particles. Besides the JKR theory, other contact models have been proposed. The Derjaguin–Muller–Toporov (DMT) theory is another contact model [16]; it is suitable for small particles and assumes that adhesive forces act around the rim of the contact area between the particles. The Maugis–Dugdale solution was proposed for medium-sized particles [17,18]. Several previous studies indicated that although these models describe the basic contact process, their treatments of energy dissipation are insufficient. In particular, a study using molecular dynamics simulations showed that the kinetic energy of the macroscopic particles is converted into molecular motions, which results in more energy dissipation than in the JKR theory [19]. Other molecular dynamics simulations of head-on collisions between nonadhesive particles demonstrated that plastic deformation of the particles results in the dissipation of kinetic energy, and they also obtained the yield velocity at which the plastic deformation begins [20,21]. Molecular motion and particle deformation result in energy dissipation and affect the physical processes of the powder

_____

*Contact author: yoshida.yuki.astpl@gmail.com

system, but these effects are not included in the contact models listed above. Krijt *et al.* [22] constructed a new dissipation model that adds the viscoelasticity of the particles and the effect of the plastic deformation to the JKR theory. Krijt *et al.* showed the validity of their model for micron-sized particles by comparing it to some experiments of collisions with impact velocities lower than a few percent of sound velocities. It is necessary to check the validity of their model through microscopic molecular dynamics simulations.

Some contact models do include particle deformation and molecular motions. For example, crack propagation in the contact area due to the molecular motion has been studied [23]. Dissipation forces due to the viscoelastic deformation were also considered [22,24]. The contact models that include these effects are consistent with experiments on collisions between particles larger than a few μm in size (e.g., Refs. [22,25,26]). However, their validity for smaller particles has not yet been confirmed. Molecular dynamics simulations are particularly useful to clarify the actual particle interactions for such small particle sizes.

Molecular dynamics (MD) simulations are used to study the physical processes involved by analyzing molecular motion. In other words, MD simulations are molecular N-body simulations. Such MD simulations have been used primarily in engineering, biology, and even in the study of particle contact dynamics. In particularly, collisions between nanoparticles have been well investigated (e.g., Refs. [27–36]). Collisions between a nanoparticle and an atomic cluster were also simulated, and their rebound or adhesion was studied [37]. Nietiadi *et al.* [29,34] simulated the collisions between silica nanoparticles with an impact velocity of less than 1000 m/s and investigated the COR and bouncing threshold. They used Si and O atoms to model the silica nanoparticles, and covalent bonds bind these atoms. Most of these studies focused on high-velocity collisions of nanoparticles with impact velocities exceeding 1000 m/s, about 20% of the sound velocity, to investigate particle melting and fragmentation, which is beyond the scope of contact models. Although there have been few MD simulation studies with impact velocities of the order of tens of m/s, a few percent of the sound velocity, the validity of contact models under these conditions has not yet been confirmed. Tanaka *et al.* [19] used the Lennard-Jones potential as the interatomic potential and investigated the collisions between submicron-sized particles with an impact velocity of less than 50 m/s, assuming argon atoms. They found that the COR obtained from the MD simulations is smaller than that predicted by the JKR theory and that collisions with large velocities cause strong deformation and energy dissipation. Nietiadi *et al.* [29,35] investigated the collisions between nanoparticles of radii less than 20 nm. In this way, the previous studies mainly simulated collisions between nanoparticles with a radius on the order of 10 nm, consisting of several million molecules, and since low collision velocities result only in coalescence, they investigated collision velocities with about 10% of the sound velocity, although such collision processes cannot be described by the contact model presented above. As the particles become larger, they start to bounce back even at a few percent of the sound velocity, and such a collision process can be compared to the contact model. To validate the model, we should use particles of about 100 nm or less, where

bouncing occurs. Here, we use MD simulations to explore the realistic particle interactions with submicron particles at impact velocities of around 100 m/s. We have also developed a new contact model with dissipation that can reproduce MD simulations.

In this paper, we study particle collisions using MD simulations. The JKR theory and a dissipative model of Krijt *et al.* [22] are first introduced in Sec. II because the JKR theory is often used in the powder simulations and the dissipative model is an extended model of the JKR theory. We next explain our simulation method, the particle models, and the initial condition of the collisions in Sec. III. In Sec. IV, we present the results of the MD simulations in which particle interactions and the coefficient of restitution are investigated. Based on these results, we construct new contact models in Sec. V. Finally, we summarize our results and discuss future work in Sec. VI.

II. CONTACT MODEL

A. Hertz theory

In this section, we first explain the models of the interaction between two elastic spheres in contact. We start with the Hertz theory. We consider two particles with radii R_1 and R_2. They have Young's moduli E_1 and E_2, Poisson's ratios ν_1 and ν_2, and masses m_1 and m_2. We introduce the reduced particle radius $1/R^* = 1/R_1 + 1/R_2$, the reduced Young's modulus $1/E^* = (1 - \nu_1^2)/E_1 + (1 - \nu_2^2)/E_2$, and the reduced mass $1/m^* = 1/m_1 + 1/m_2$. When the spheres are in contact, the contact surface can be treated as a disk with radius a. The mutual approach δ is the compression length given by

$$\delta = R_1 + R_2 - X, \tag{1}$$

where X is the distance between the centers of the two particles. In the Hertz theory, connection and disconnection occur at $\delta = 0$; thus, δ is positive for particles in contact.

The Hertzian force can be written as follows:

$$F_{\mathrm{H}} = \frac{4E^*a^3}{3R^*}, \tag{2}$$

where the radius of the contact surface between the two particles, a, is given by $\sqrt{R^*\delta}$ in the Hertz theory. The Hertzian force is always repulsive and nonadhesive, as a positive force denotes a repulsive one. The forces are identical in both the loading and unloading phases, and there is no hysteresis. As a result, the coefficient of restitution is always $e = 1$ in the Hertz theory. We can also obtain the Hertzian potential energy by integrating Eq. (2):

$$U_{\mathrm{H}} = \frac{8E^*}{15}R^{*1/2}\delta^{5/2}. \tag{3}$$

The pressure at the center of the contact area increases with δ and is given by

$$p_{\mathrm{c,H}} = \frac{2E^*}{\pi}R^{*-1/2}\delta^{1/2}. \tag{4}$$

B. Johnson–Kendall–Roberts theory

In the JKR theory [11,15], δ and a are related as

$$\delta R^* = a^2 - \sqrt{\frac{4\pi \gamma a R^{*2}}{E^*}}, \tag{5}$$

where γ is the surface energy per unit area [38]. The contact radius is obtained from this equation as a function of δ. The force between the particles is given by

$$F_{\mathrm{J}} = \frac{4E^* a^3}{3R^*} - \sqrt{16\pi \gamma E^* a^3}. \tag{6}$$

A positive value of F_{J} again indicates a repulsive force, whereas a negative one indicates an attractive force. The potential energy in the JKR theory can be written as follows:

$$U_{\mathrm{J}} = a^3 E^* \left[\frac{1}{5}\left(\frac{a}{R^*}\right)^2 - \frac{2}{3}\frac{\delta}{R^*} + \left(\frac{\delta}{a}\right)^2 \right] - 2\pi \gamma a^2. \tag{7}$$

This equation consists of two terms: the first represents the elastic potential energy, and the second represents the surface energy. The maximum absolute value of the attractive force between the two contacting particles, F_c, is given by $3\pi \gamma R^*$, and it occurs at $\delta = -0.397\delta_0$, where δ_0 is the stationary mutual approach. The stationary point exists where $F_{\mathrm{J}} = 0$ and is denoted by the subscription 0. The stationary contact radius a_0 and the stationary mutual approach δ_0 are given by

$$a_0 = \left(\frac{9\pi \gamma R^{*2}}{E^*}\right)^{1/3}, \quad \delta_0 = \frac{a_0^2}{3R^*}. \tag{8}$$

The pressure at the center of the contact area is given

$$p_{\mathrm{c,J}} = \frac{2E^* a}{\pi R^*} - \sqrt{\frac{4\gamma E^*}{\pi a}}. \tag{9}$$

In the JKR theory, contact between the two particles starts at $\delta = 0$, and the disconnection occurs at $\delta \simeq -0.825\delta_0$. The difference in δ between the connection and disconnection represents hysteresis, which indicates energy dissipation in the amount of $\simeq 0.773 F_c \delta_0$ [39], which gives the coefficient of restitution in the JKR theory.

C. Krijt model

The contact model of Krijt *et al.* [22] (hereafter referred to as the Krijt model) includes two energy dissipation mechanisms. One is the bulk dissipative force due to the viscoelasticity [24,40]. The other is a delayed evolution of the contact radius based on the viscoelastic crack theory [23].

In the Krijt model, the interaction force between two particles in contact consists of two components, and the equation for relative motion is given by

$$m^* \frac{d^2\delta}{dt^2} = -(F_{\mathrm{E}} + F_{\mathrm{dis,K}}), \tag{10}$$

where F_{E} is the elastic force and $F_{\mathrm{dis,K}}$ is the dissipative force:

$$F_{\mathrm{E}} = \int_0^a 2\pi r p(r)\, dr, \tag{11}$$

$$F_{\mathrm{dis,K}} \simeq \frac{T_{\mathrm{vis}}}{v^2} \int_0^a 2\pi r \dot{\delta} \frac{\partial p(r)}{\partial \delta}\, dr = \frac{2T_{\mathrm{vis}} E^*}{v^2} a\dot{\delta}, \tag{12}$$

where $p(r)$ is the pressure distribution across the contact area [22,41] and T_{vis} is the relaxation time [24,40]. Since $p(r)$ depends on both δ and a, the elastic force F_{E} has hysteresis due to the delayed evolution of a. Some studied suggested that T_{vis} is approximately proportional to the particle radius [22,42]. We should note that the dissipation force $F_{\mathrm{dis,K}}$ has the opposite sign to the relative velocity dX/dt because $\delta = R_1 + R_2 - X$. Thus, this dissipation force acts in the same way as a viscous resistance.

To describe the evolution of the contact radius, the Krijt model uses the Griffith theory [43] instead of Eq. (5). The Griffith theory describes the crack propagation and gives the rate of evolution of the contact radius, $\dot{a}$, which is proportional to $1/T_{\mathrm{vis}}$. The detailed formula for $\dot{a}$ is presented in Appendix B. The viscoelastic effect in crack propagation results in a delay in the evolution of a compared with that given by Eq. (5) and causes hysteresis in the evolution of the contact radius and the elastic force F_{E} between loading and unloading phases (e.g., Refs. [22,44]). In our MD simulations for nano- and submicron-sized particles, however, we find that the hysteresis of F_{E} due to the delayed a is much smaller than that of the dissipative force $F_{\mathrm{dis,K}}$.

Given the initial conditions of the collision, the outcome of the collision can be obtained by numerically solving Eq. (10). Krijt *et al.* incorporated the plastic deformation model of Thornton and Ning [45] into the outcome to obtain a coefficient of restitution e that includes the effects of plastic deformation. The plastic deformation of the Thornton and Ning model with $v_{\mathrm{imp}} > v_Y$ results in a decrease in e, as expressed by the following equation:

$$e_{\mathrm{TN}} = \left(\frac{6\sqrt{3}}{5}\right)^{1/2} \sqrt{1 - \frac{v_Y^2}{6v_{\mathrm{imp}}^2}} \left[1 + 2\sqrt{\frac{6v_{\mathrm{imp}}^2}{5v_Y^2} - \frac{1}{5}} \right]^{-1/4}, \tag{13}$$

where v_Y is the yield velocity, which is the impact velocity at which the plastic deformation begins, and $\hat{v} = v_Y/v_{\mathrm{imp}}$. Takato *et al.* [20] performed MD simulations of collisions between nonadhesive particles and estimated $v_Y \simeq 26.1$ m/s for $R > 15$ nm for Argon particles. Krijt *et al.* combined e obtained by numerically solving Eq. (10) with the energy dissipation due to plastic deformation in the Eq. (13) and obtained the coefficient of restitution e_{pl} including the effect of plastic deformation as

$$e_{\mathrm{pl}} = \sqrt{e^2 - \left(1 - e_{\mathrm{TN}}^2\right)}. \tag{14}$$

III. METHODS

We have simulated the head-on collisions between two equal-mass particles using the MD simulation code LAMMPS [46]. The particles are spheres consisting of 12–6 Lennard–Jones (LJ) atoms arranged in a face-centered cubic (fcc) structure. The LJ atoms are subject to the potential $u(r_{ij}) = 4\epsilon\{(r_{ij}/\sigma)^{-12} - (r_{ij}/\sigma)^{-6}\}$, where r_{ij} is the distance between the ith and jth atoms, ϵ is the potential depth, and σ is the distance at which $u(r_{ij}) = 0$. We normalize the parameters using σ, ϵ and the molecular weight, thus expressing them in so-called LJ units. For example, the unit of temperature is

TABLE I. A table of the LJ units for Argon [47], water [48], and Ag [49]. Time and velocity of the LJ units are $t = \sigma\sqrt{m/\epsilon}$ and $v = \sqrt{\epsilon/m}$.

	m (g/mol)	σ (nm)	ϵ (meV)	t (ps)	v (m/s)
Ar	39.95	0.341	10.32	2.16	158
H_2O	18.02	0.319	53	0.599	533
Ag	107.87	0.2644	345	0.476	555

ϵk_B^{-1}, where k_B is the Boltzmann constant and $k_B = 1$ is set in the LJ units. We prepare a population of molecules arranged in an fcc structure and cut the molecules outside a certain distance from the origin to form a sphere. The number of atoms N in a particle is from $N \simeq 1.1 \times 10^5$ to $N \simeq 1.2 \times 10^8$. The particle density is $\rho \simeq 1.09 m\sigma^{-3}$. The particle temperature T is determined by giving random motion to the atoms: $T = 2E_{kin}/3N$ where $E_{kin} = \sum_i^N m_i v_i^2/2$, m_i and v_i are the mass and velocity of the ith atom. The initial particle temperature is set to $T = 10^{-6}\epsilon k_B^{-1}$ in the canonical ensemble (NVT), corresponding to, for example, 8×10^{-5} K for argon. In this paper, we treat the collisions with extremely low temperatures as a first step. We place two particles at a distance greater than $r_{cut} = 5\sigma$ from each other and give an initial velocity for each particle so that they collide head-on. The orientations of each particle are randomly rotated. We also vary the impact velocity from $v_{imp} = 0.04$ to 0.50. We adopt a cutoff distance for the interaction for all atoms at $r_{cut} = 5.0\sigma$ and perform the simulations in the microcanonical ensemble (*NVE*) for a time of at least 3×10^4 with a timestep of 2^{-7} in the LJ units. The positions and velocities of molecules are updated by the Velocity Verlet algorithm.

We introduce examples of LJ units for three atoms, shown in Table I. The LJ lengths are almost the same, and the particle radius corresponds to 10–100 nm. Water molecules have a complex potential. Note that the normalizing parameters of water molecules are quantitatively different by a factor of several.

By simulating a Hertzian contact, we next determine the particle radius $R(= R_{1,2})$ and the reduced Young's modulus E^*. In the Hertz theory, there are no adhesive forces between particles. To simulate a Hertzian contact, we therefore remove the attractive term $-(r/\sigma)^{-6}$ between atoms belonging to different particles. By fitting to the Hertzian force, we can obtain R and E^*, which we represent in Table II. The fitting procedures are shown in Appendix A. A previous simulation investigated the elastic constant of FCC LJ solid and showed $E^* \simeq 34.7\epsilon/\sigma^3$ [50]. Their obtained E^* is smaller than that

TABLE II. The particle radius R and the reduced Young's modulus E^* in the LJ units.

N	R	E^*
113 637	29.6	53.2
914 443	58.9	58.4
3 120 599	88.4	63.7
14 434 147	147	65.5
115 506 757	294	68.3

of our MD simulations due to their shorter cutoff length than ours. We adopt the surface energy as $\gamma = 3.17$ and Poisson's ratio $\nu = 0.25$. The surface energy of the particle is derived as discussed in Appendix C. The sound velocity of the particles is calculated as $V \simeq \sqrt{E/\rho} \sim 11$. In this paper, we mainly treat the impact velocities less than a few % of the sound velocity ($v_{imp} \lesssim 0.3$).

IV. RESULTS

A. Interparticle force

1. Hysteresis

We show an example of collision simulation with $R = 147\sigma$ and $v_{imp} = 0.10(\epsilon/m)^{1/2}$ in Fig. 1. The particle radius and impact velocity correspond to 50 nm and 15–50 m/s, respectively, in the physical units. We always use the LJ units, although we omit the symbols such as σ and ϵ from now on. From left to right, the panels show the particles in the initial stage, during the contact, and after the disconnection. After disconnection, the surfaces become rough because of the displacement of atoms. We calculate the center of mass of each particle and derive its velocity and acceleration by differentiating it with respect to time. The interparticle force is then obtained by multiplying the acceleration by the particle mass.

Figure 2 shows the interparticle force as a function of δ. The red curve shows the case illustrated in Fig. 1, the gray curves show the results obtained with different crystal orientations, and the dotted line shows the JKR theory. The unstable solution of the JKR theory is omitted in the figure since it is not stably realized in the actual contact process. In the JKR theory, the two particles are in contact at $(\delta, F) = (0, -8F_c/9) \simeq (0, -1950)$, disconnected at $(\delta, F) = [-(3/4)^{2/3}\delta_0, -5F_c/9] \simeq (-1.33, -1220)$, and are in the stationary state at $(\delta, F) = (\delta_0, 0) \simeq (1.61, 0)$ for $R = 147$. The maximum attractive force is $F_c = 3\pi\gamma R^* \simeq 2200$ for $R = 147$. The JKR force in both the loading and unloading phases follows the same curve, although the moments of connection and disconnection are different; this represents the hysteresis in the JKR theory. The two particles first approach each other, represented by increasing δ. A negative force acts on them when they come into contact because of the attractive molecular force. As they are compressed, the repulsive force increases with increasing δ, which is the loading phase. After the greatest compression, the two particles rebound, and δ decreases; this corresponds to the unloading phase. For δ becomes $\delta < -(3/4)^{2/3}\delta_0$, the disconnection of the contact occurs; otherwise, the two particles coalesce, oscillating between loading and unloading.

In all the MD simulations, we find a difference between the loading and unloading phases, which is the hysteresis in the MD simulations. The example case discussed above has the largest hysteresis among eight runs. The collisional process depends on the orientations of each particle, and particles easily stick to each other when their orientations are similar [35]. Although the force in the loading phase agrees with the JKR theory, the force in the unloading phase differs from that in the loading phase. Figure 2 shows that hysteresis shifts the mutual approach δ toward larger δ in the unloading
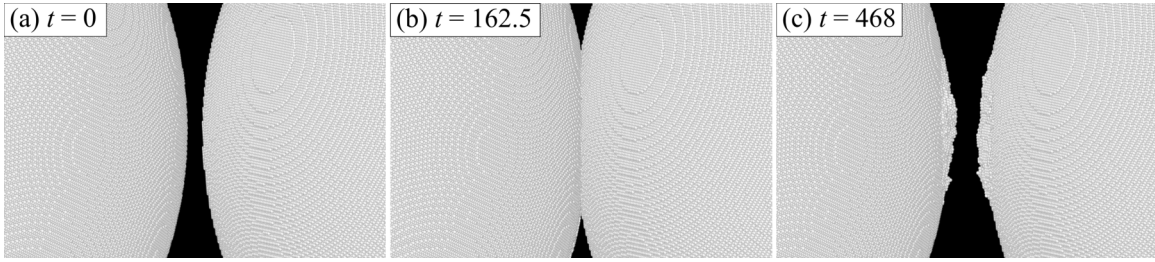
FIG. 1. Snapshots of particles with $R = 147$ during a collision with $v_{\mathrm{imp}} = 0.10$ (a) the initial stage, (b) at the highest compression, and (c) after disconnecting. These figures are visualized by OVITO [51].

phase. Particle kinetic energy is dissipated by the area enclosed by the loading and unloading curves. We note that the total energy of the molecular system is conserved. The kinetic energy of particle translational motion is converted to the internal energy of particles. The energy conversion is discussed in detail in Sec. IV C.

2. Dependence on particle radius and impact velocity

Figure 3 shows the interparticle force as a function of δ for all radius cases with $v_{\mathrm{imp}} = 0.06$ and 0.10. The particles coalesce for $R \leqslant 88.2$, and the force oscillates at a δ larger than in the JKR theory. For $R = 29.6$, the force paths of the loading and unloading phases are distinctly different and the force finally oscillates at $\delta \simeq 2$, which indicates the occurrence of the plastic deformation. Focusing on the force difference between the loading and unloading phases normalized by F_c, we see that it is about F_c for $R = 29.6$ and about 3–4 times as large as F_c for $R = 294$. This trend is roughly consistent with the relationship $F_{\mathrm{dis,K}}/F_c \propto R^{1/2}$ as $F_{\mathrm{dis,K}} \propto aT_{\mathrm{vis}} \propto R^{3/2}$ and $F_c \propto R$, where we approximate $a \propto R^{1/2}$, if the hysteresis comes from the dissipative force of the Krijt model. As the radius increases, the difference in force normalized by F_c also
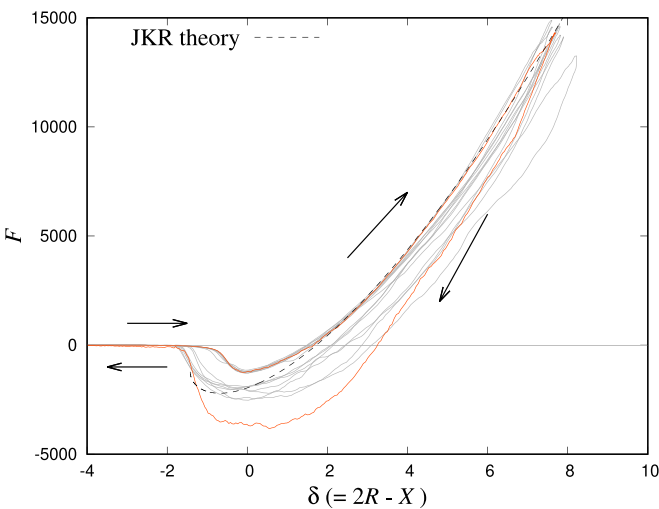
increases. However, the effect of hysteresis becomes smaller as the radius increases since the kinetic energy, which is inertia, is proportional to R^3.

Figure 4 shows the interparticle force as a function of δ normalized by F_c and δ_0 for all radius cases with $v_{\mathrm{imp}} = 0.20$ and 0.50. The hysteresis is clearly apparent in Fig. 4. Higher impact velocities cause significant shifts in δ in the unloading phase, resulting in stronger hysteresis. The significant shifts in δ for $v_{\mathrm{imp}} \geqslant 0.2$ indicate plastic deformation. In all radius cases, the particles coalesce for $v_{\mathrm{imp}} = 0.50$ with the remaining at large δ, which suggests strong plastic deformation. Though this figure shows the collision results with a particular orientation, such large shifts in δ occur and particles stick even for other orientations.

Figures 5(a) and 5(b) show images of particles with $v_{\mathrm{imp}} = 0.10$ and 0.50 at the ends of the simulations for $R = 88.4$. The particles remain spherical for $v_{\mathrm{imp}} = 0.10$. In contrast, a bump is formed on the particle surface, and the contact area is increased for $v_{\mathrm{imp}} = 0.50$. This deep sticking causes a significant shift in δ in the unloading phase. The bump on the right-most particle in Fig. 5(b) is called an antipodal deformation. The atoms are pushed from the contact area to the opposite surface, forming the bump. Figure 5(c) shows the atoms that do not arrange in an FCC lattice structure, indicating cracks in the particles. The cracks are seats and extend from the contact surface in a planar state, which can be observed as the crack lines on the surface in Fig. 5(b). In particular, the crystal structure around the contact surface is extremely broken.

3. Plastic deformation

Plastic deformation occurs due to stress acting on the contact area. The interparticle force in Figs. 3 and 4 shows possible plastic deformation at all impact velocities for $R = 29.6$ and at all radii for $v_{\mathrm{imp}} = 0.2$. In this section, we estimate the pressure and verify whether it is sufficient to cause plastic deformation.

The onset of plastic deformation is determined by the yield strength Y. Takato *et al.* [20] performed MD simulations of collisions between nonadhesive particles and found a yield velocity of $v_Y \simeq 0.17$ for $R > 44$, which corresponds to $Y = 0.15E^*$. However, the yield strength Y is theoretically given as $Y \lesssim 0.38E^*$ for defect-free material [22,52]. Spheres begin to deform plastically when the pressure at the center of the contact area reaches $p_c = 1.6Y$ [15]. Then, the plastic deformation of particles is expected to occur for $p_c \geqslant 0.24E^*$ numerically and $p_c \geqslant 0.6E^*$ theoretically. We compare these

FIG. 2. Interparticle force with $R = 147$ as a function of δ for $v_{\mathrm{imp}} = 0.10$. The black dotted curve is the JKR theory, the red curve shows the example run, and the gray curves show the other runs with different crystal orientations. The arrows show the time evolution of the force. The force and the length of the mutual approach are plotted in the LJ units.
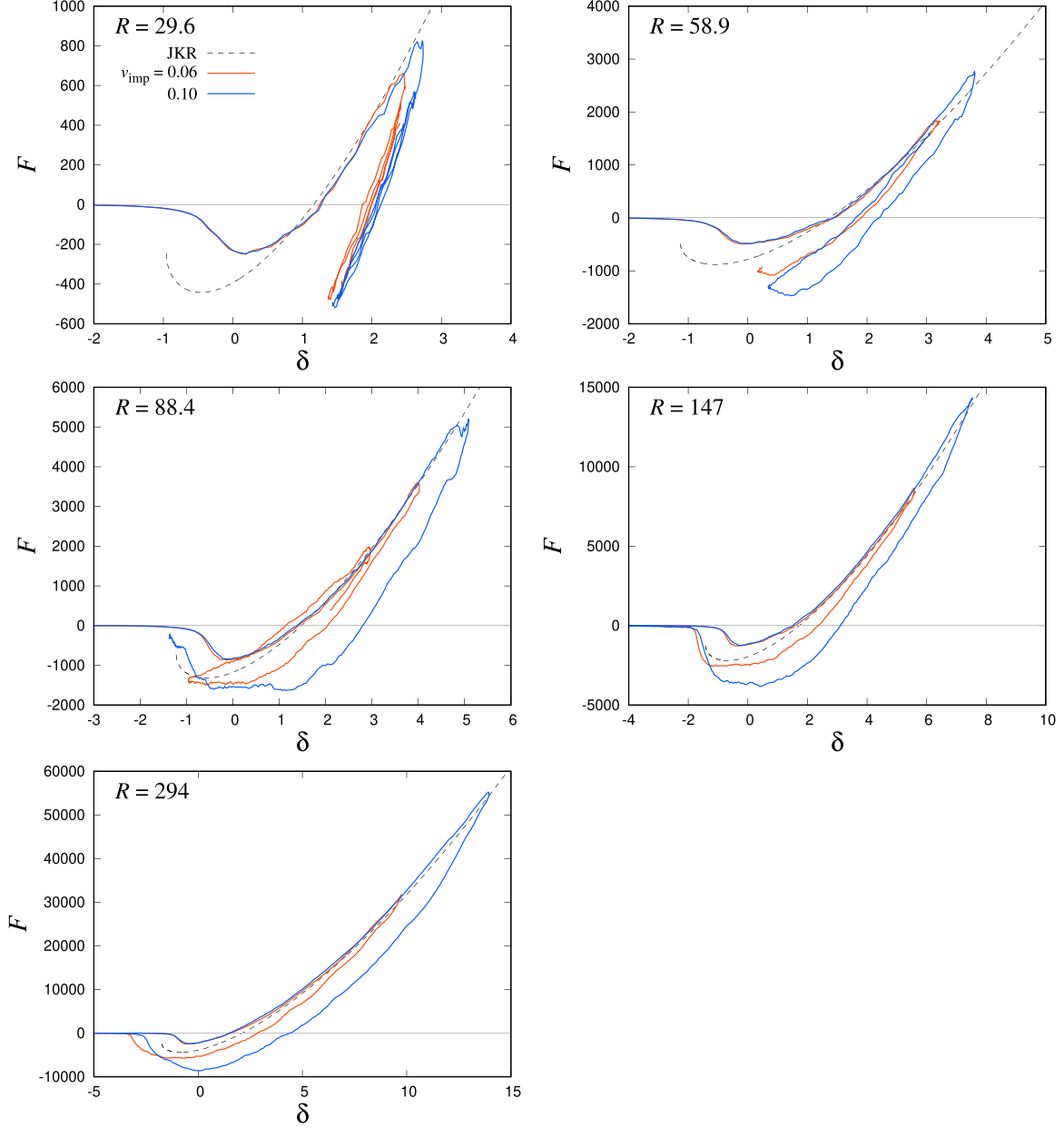
FIG. 3. Interparticle force as a function of δ with $v_{imp} = 0.06$ and 0.10. The black curves represent the JKR theory. The force and the length of the mutual approach are plotted in the LJ units.

values with maximum pressures between particles in our MD simulations.

The pressure at the center of the contact area can be estimated by Eq. (4). Since from the energy conservation, the initial kinetic energy equals the Hertzian potential energy of Eq. (3) at the maximum compression, the maximum δ can be estimated as

$$\delta_{\max} = \left(\frac{15}{32} \frac{m v_{imp}^2}{E^* R^{*1/2}} \right)^{2/5}. \tag{15}$$

Combining Eqs. (4) and (15), we can estimate the maximum pressure as $p_{c,H} \simeq 0.26 E^*$ for $v_{imp} = 0.20$. We note that the estimated maximum pressure using the Hertz theory does not depend on the particle radius. For small particles, the Hertz

theory underestimates $\delta_{\max}$ and p_c, and the JKR theory estimates them more accurately; for $v_{imp} = 0.06$, $p_{c,J} \simeq 0.29 E^*$, with $R = 29.6$.

The pressure estimated above is less than the theoretical onset pressure of plastic deformation ($0.6E^*$) but larger than that obtained by the previous MD simulation. The displacement of δ shown in Figs. 3 and 4 indicates the occurrence of the plastic deformation. Therefore, in this study, we use their onset pressure of plastic deformation.

4. Contact radius

We calculate the contact radius using the gyration radius derived from the molecule distribution in a thin layer of the thickness 1σ containing the contact surface. Let $\boldsymbol{r}_i$ be
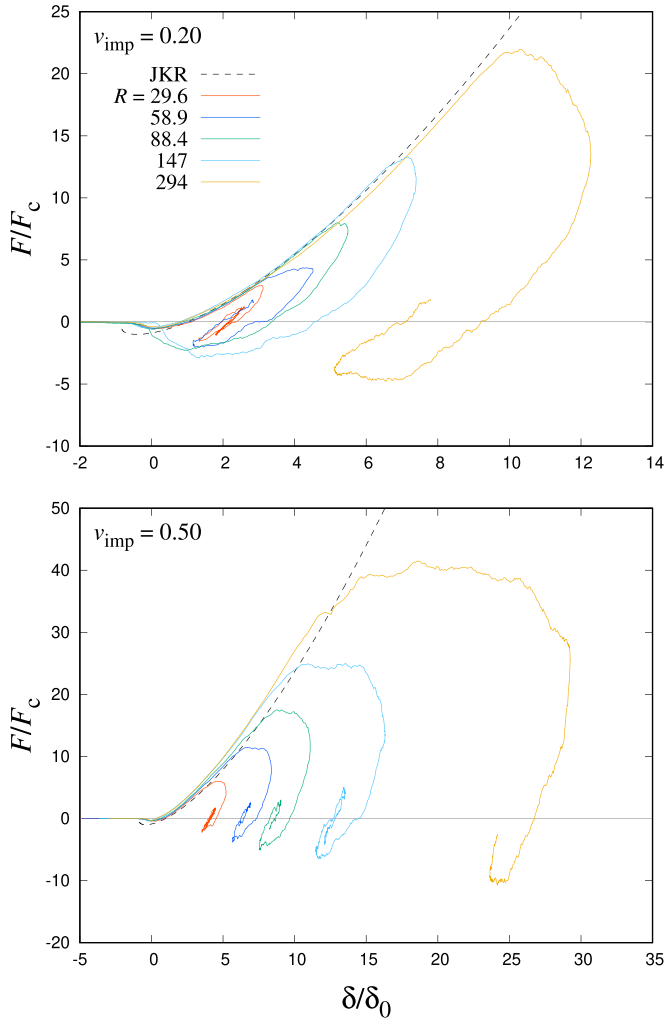
FIG. 4. Normalized interparticle force as a function of δ/δ_0 with $v_{\mathrm{imp}} = 0.20$ and 0.50.

FIG. 5. Images of particles of $R = 88.4$ with (a) $v_{\mathrm{imp}} = 0.10$ and (b) $v_{\mathrm{imp}} = 0.50$ at the end of simulations. Panel (c) shows the results of dislocation analysis of panel (b) and red atoms show those that do not have an FCC lattice structure due to molecular movement by collision.

the position vectors projected onto the contact surface for molecules in this layer. The gyration radius is given by $r_{\mathrm{g}} = \sqrt{\sum_i |\boldsymbol{r}_i - \boldsymbol{r}_{\mathrm{M}}|^2/n}$, where $\boldsymbol{r}_{\mathrm{M}}$ and n are the position of the center of mass and number of the molecules in the layer, respectively. Then, we obtain $a = \sqrt{2} r_{\mathrm{g}}$. Figure 6 shows the contact radius as a function of δ for $R = 88.4$. The contact radius of the MD simulations is smaller than that of the JKR theory in the loading phase and larger in the unloading phase, indicating the delayed a and the hysteresis. The hysteresis of a in the MD simulations is larger than that of the Krijt model, although the behavior of the contact radius evolution is similar to that of the Krijt model.

For the high-velocity collisions of $v_{\mathrm{imp}} \geqslant 0.2$, the contact radius increases around the most compressed point. For $v_{\mathrm{imp}} = 0.5$, the contact radius increases significantly around the most compressed point due to plastic deformation (see Fig. 6). Such an effect of plastic deformation is not considered in the JKR theory.

In the crack propagation model (e.g., Refs. [22,23]), a is delayed due to the viscoelasticity, but the degree of delay predicted by the model is insufficient compared to that in the MD simulations. The model has the uncertainty of the
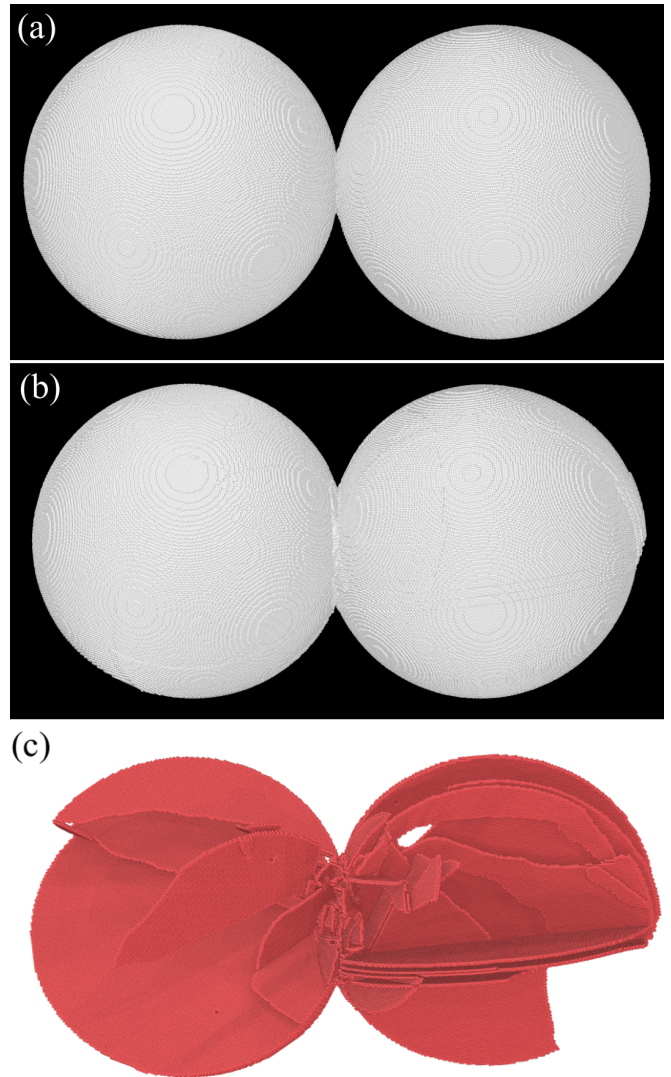
relaxation time T_{vis}, which may cause the deference between the MD simulations and the model.

B. Coefficient of restitution

1. Dependence on the impact velocity

The coefficient of restitution (COR) e provides an appropriate method for evaluating the effects of the kinetic energy dissipation of the translational motion. Figure 7 shows the COR for $v_{\mathrm{imp}} = 0.06, 0.10$ and 0.20 for particles with $R = 147$. A previous study suggested that the crystal orientation within the particles may significantly affect the collision results [35], consistent with Fig. 7. Figure 7 also shows that the COR of the MD simulations is smaller than that obtained from the JKR theory. As shown in Sec. IV A, the hysteresis is larger for collisions with higher impact velocities, which leads to larger energy dissipation and smaller values of e.
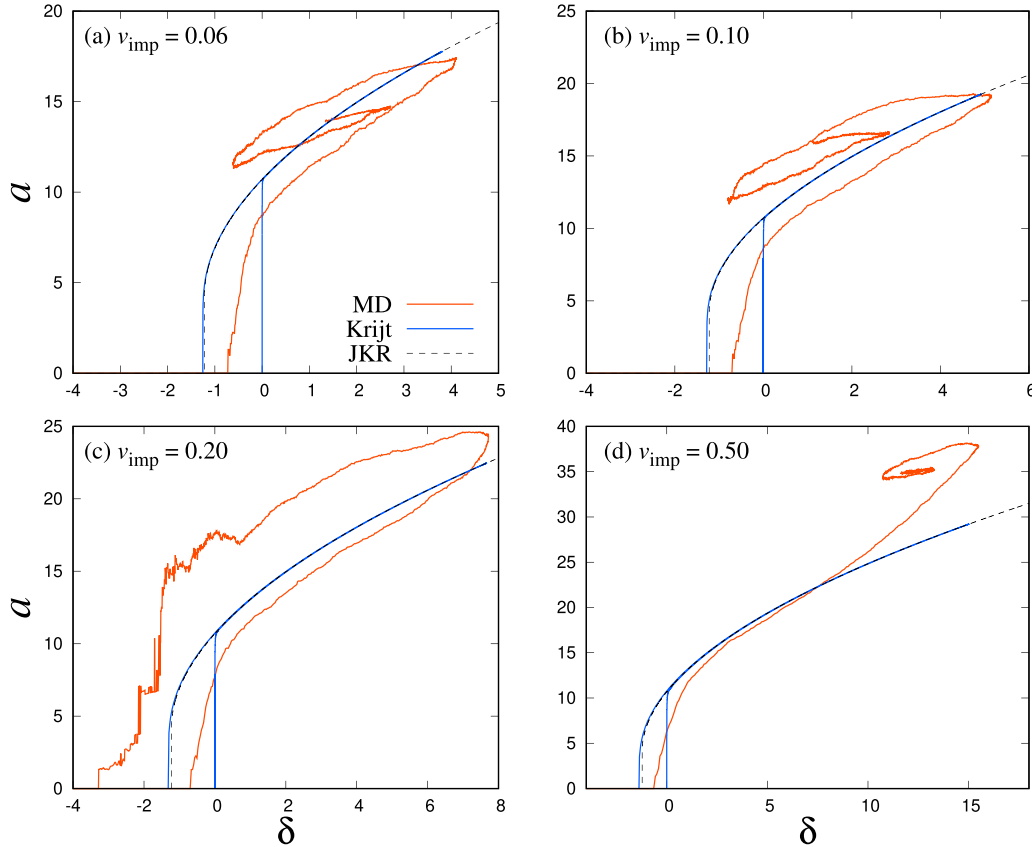
FIG. 6. Contact radius as a function of δ for $v_{imp} = 0.06,\ 0.10,\ 0.20,$ and 0.50 with $R = 88.4$. The black dotted curves show the JKR theory, the red curves show the MD simulations, and the blue curves show the Krijt model with $T_{vis} = 0.075$, respectively.

Since the energy dissipation is independent of the impact velocity in the JKR theory, e approaches 1.0 as the impact velocity increases. The Krijt model predicts larger energy dissipation than does the JKR theory because it includes the energy dissipation due to the hysteresis described in Sec. II C. In Fig. 7, we set $T_{vis} = 0.075$ to fit the MD results with $v_{imp} = 0.06$. This model can also reproduce the MD results for $v_{imp} = 0.10$ within the error bars, although it does not match for $v_{imp} = 0.20$. This occurs because high-velocity collisions have large hysteresis, as shown in Fig. 4, causing e to decrease as the impact velocity increases. A stronger energy dissipation occurs in the MD simulations than that caused by the model of plastic deformation.

Here, we compare our MD simulations with previous studies for velocity dependence. Nietiadi *et al.* [29] treated silica particles of 10–20 nm radius. In their results, the COR e has a peak similar to our MD simulations, but the peak is located where v_{imp} is 5–8% of sound velocity, which is several times as large as that of our results, about 1% of sound velocity. This difference is thought to be due to the difference in potentials: silica has covalent bonds and spherically asymmetric potential, whereas LJ atoms have noncovalent bonds and spherically symmetric potential. The LJ atoms tend to move tangentially to the contact surface and deform easily even at low impact velocities, and translational energy is easily converted to kinetic energy of atomic random motion. Therefore, the impact velocity where e peaks in our simulations is smaller than that of previous studies. Nietiadi *et al.* [35] used LJ atoms

as we do and examined e for $R < 90$ and showed the peak of e at the same impact velocity. Tanaka *et al.* [19] examined the coefficient of restitution for $R \simeq 88$ only, and their results are consistent with that of this study. Few previous studies examined the particle collisions with $R > 100$ and thus cannot be compared to our results. Our results indicate a strong dependence of the translational kinetic energy dissipation on the radii for $29 < R < 150$.

2. Dependence on radius

Figure 8 compares the COR obtained for $R = 58.9, 88.4, 147$ and 294 as a function of v_{imp} with the results from the JKR theory and the Krijt model. For $R = 29.6$, all particle collisions result in coalescence. In the JKR theory, the collisions result in energy dissipation of $\simeq 0.773 F_c \delta_0 \propto R^{4/3}$, which means that collisions with smaller particles result in smaller e because the translational kinetic energy is proportional to R^3. In the MD simulations, e decreases, and its deviation increases as the radius decreases. As shown in Fig. 3, the hysteresis is larger for smaller radii and higher impact velocities, which explains the trend of the COR in Fig. 8.

The coefficient of restitution e obtained by the MD simulations for $R = 88.4$ is the same as Tanaka *et al.* [19]. Nietiadi *et al.* [29,34] also found that e has the peak and weakly depends on the particle radius for radii between 10–20 nm, which corresponds to $R \simeq 30$ and 60 in the LJ units. However,
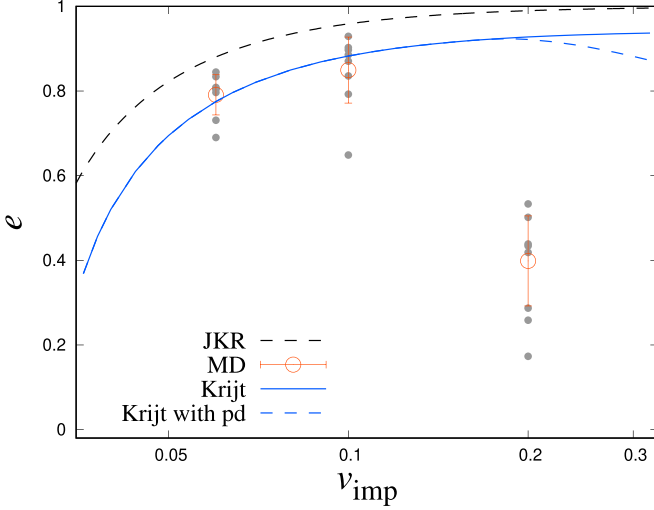
FIG. 7. Coefficient of restitution for $v_{\text{imp}} = 0.06, \ 0.10,$ and 0.20 with $R = 88.4$. The gray points are the results of eight runs with different crystal orientations, and the red points with error bars are the root mean square (RMS) of the 8 results with their deviations. The dashed black and solid blue curves show the JKR theory and the Krijt model with $T_{\text{vis}} = 0.075$, respectively. The dashed blue curve shows the Krijt model with plastic deformation (pd) for $Y = 0.12E^*$ based on the model of Thornton and Ning [45].

our MD simulations show that the results of collisions with $R = 29.6$ and 58.9 are quite different; all collisions with $R = 29.6$ result in coalescence while e reaches ~ 0.3 for $R = 58.9$. The difference between the previous studies and our study comes from the interaction of molecules consisting of particles. The previous studies used silica nanoparticles in which covalent bonds bond Si and O atoms. Such a particle is expected to be more rigid and to have a larger Young's modulus than that in particles composed of LJ atoms. Comparison to the previous studies suggests that the molecular bonds affect particle collisions well.

Figure 9 shows the sticking probability for each particle radius as a function of v_{imp}. For low impact velocities, smaller particles easily stick. The onset impact velocity for bouncing increases with decreasing particle radius. For $v_{\text{imp}} > 0.2$, the sticking probability rapidly decreases since coalescence occurs with strong energy dissipation due to plastic deformation.

3. Comparison with the Krijt model including the plastic deformation

In the Krijt model, we set the relaxation time to be $T_{\text{vis}}(R) = 0.075(R/147)$ [22]. The Krijt model agrees well with the MD results for $v_{\text{imp}} \lesssim 0.10$ with $R = 147$ and for $v_{\text{imp}} = 0.10$ with $R = 294$. For $v_{\text{imp}} \lesssim 0.08$, the Krijt model reproduces the coefficient of restitution e with $R = 88.4$ to within the error bars but not that with $R = 58.9$. In other words, the Krijt model reproduces MD results only for low impact velocities and large radii.

The Krijt model considers the effect of plastic deformation based on Thornton and Ning [45]. The plastic deformation leads to decreased e due to energy loss as shown in Eq. (13). As discussed in Sec. IV A 3, we employ $v_Y = 0.17$ obtained by Takato for the Krijt model with plastic deformation, and

plot it in Figs. 7, 8, and 11. However, as shown in Fig. 8, the energy dissipation due to the plastic deformation of the model is insufficient to reproduce the MD results although the COR of the Krijt model with plastic deformation decreases with v_{imp} for $v_{\text{imp}} \gtrsim 0.20$. The value of $v_Y = 0.17$ is estimated from the Hertz theory, and the JKR theory is expected to give v_Y just slightly smaller. Consequently, the model curves are expected to shift to the lower left. However, the shift is not enough to be consistent with the MD simulations although the shift increases with decreasing particle radius. Even when the impact velocity is near or less than the onset velocity of the plastic deformation, more dissipation of the translational kinetic energy occurs in the MD simulations. In particular, the energy dissipation strongly depends on the particle radius and the Krijt model does not fit with this radius dependence. The results of this study indicate that collisions between particles with adhesion result in additional dissipation compared to the previous MD studies using particles without adhesion.

C. Energetics

In molecular systems, the total energy $K + W$ is conserved, where K and W are the kinetic and potential energies, respectively. The kinetic energy can be divided into $K = K_p + K_t$, where K_p is the translational kinetic energy of the macroscopic particles and K_t is the kinetic energy of random molecular motions; i.e., the thermal energy:

$$K_t = \sum_j^N \frac{1}{2} m_j (v_j - V_i)^2, \tag{16}$$

where m_j and v_j are the mass and velocity of the jth atom, and V_i is the velocity of the center of mass of the macroscopic particle to which the jth atom belongs. Because the initial temperature of the particle is close to zero, K_t at the end of each simulation is almost equal to the increase of the thermal energy ΔK_t. Bulk systems, such as those considered by the JKR theory, mainly discuss the bulk kinetic energy K_p and do not consider changes in K_t and W. Here, we investigate the energetics of collisions in the MD simulations. Figure 10 shows ΔK_t and ΔW as a function of v_{imp}. The respective energy–conversion ratios are $\Delta W/|\Delta K_p| \sim 40\%$ and $\Delta K_t/|\Delta K_p| \sim 60\%$ when particles bounce and disconnection occurs. When particles coalesce, most of K_p is converted to K_t for low impact velocities. In this case, all of K_p should be converted, but the change in W is small at low impact velocities because barely any molecular displacement occurs. Thus, the coalescence results for $v_{\text{imp}} = 0.06$ are dominated by energy conversion to K_t. However, at high impact velocities, $v_{\text{imp}} = 0.20$, the energy conversion for the coalescing case is the same as that for a case in which disconnection occurs. The particles are deformed, and sufficient molecular displacements occur to dissipate the translational kinetic energy into both the potential and thermal energies: $\Delta W/|\Delta K_p| \sim 40\%$ and $\Delta K_t/|\Delta K_p| \sim 60\%$. Assuming that the masses of the two particles after disconnection are the same as those before the collision, the kinetic–energy ratio of the particles is $K_{p,\text{end}}/K_{p,\text{ini}} = 1 - e^2$. We have confirmed that $\Delta K_p/K_{p,\text{ini}} = (\Delta K_t + \Delta W)/K_{p,\text{ini}} \simeq 1 - e^2$ in all results,
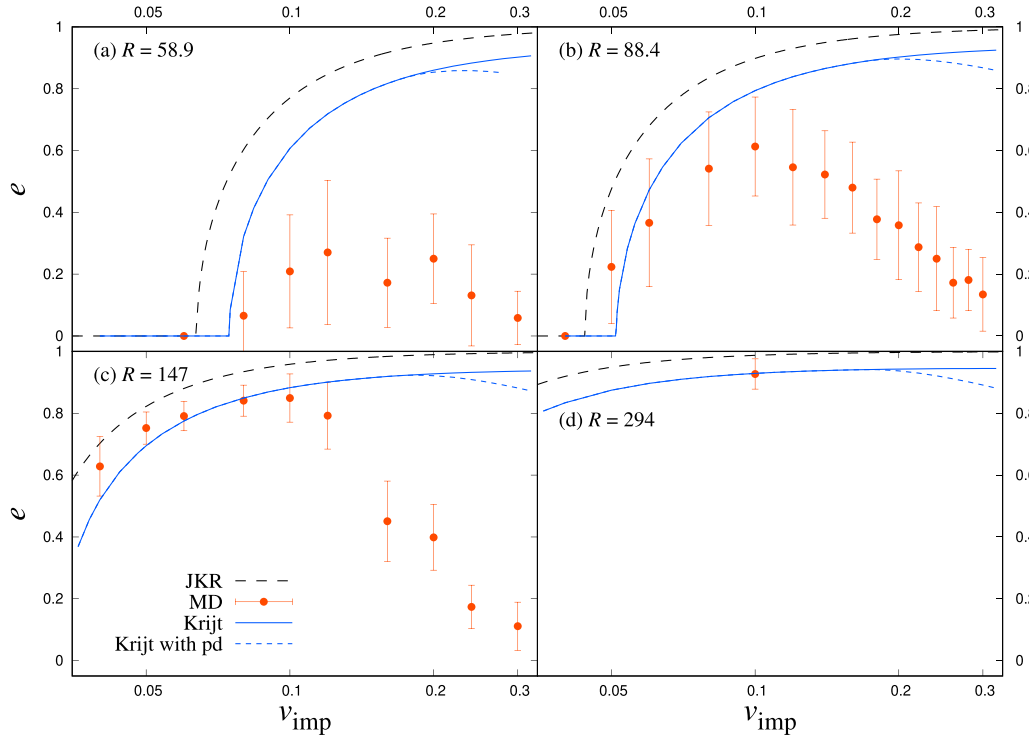
FIG. 8. Variation of the COR as a function of impact velocity. The red points with error bars are the RMS and its deviation from 20-run results with $R = 58.9$ and 88.4, and 8-run results for $R = 147$ and 294. We compare the MD results with the JKR theory (dashed black curves) and the Krijt model (solid blue curves). The dashed blue curves show the Krijt model with plastic deformation (pd) for $Y = 0.12E^*$. The relaxation time is $T_{vis}(R) = 0.075(R/147)$, which is linear with respect to the particle radius.

which means that fewer molecules move between the particles and that the particle masses before and after the collisions are approximately the same.

V. NEW DISSIPATION MODELS

As shown in Sec. IV B, our MD simulations of particle collisions have stronger energy dissipation than those predicted either by the JKR theory or the Krijt model. In particular, for high impact velocities with $v_{imp} > 0.1$ and for small particles with $R \lesssim 58.9$, the CORs are much smaller than those predicted by the Krijt model. Here, we propose two new dissipation models that reproduce the energy dissipation in our MD simulation results.
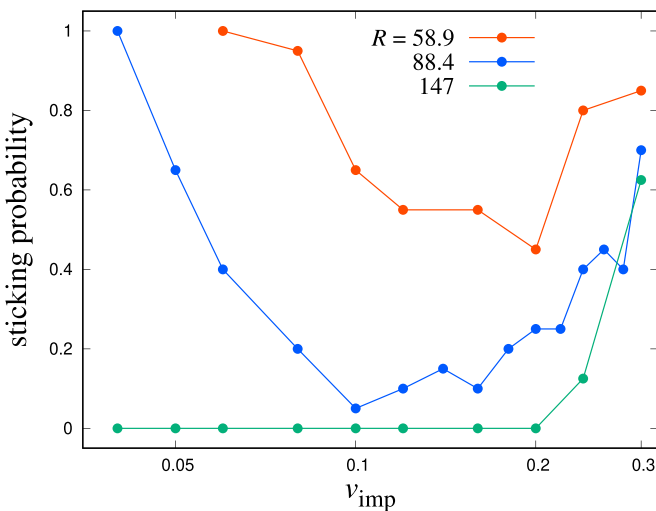

FIG. 9. Sticking probability as a function of the impact velocity for each particle radius, which is calculated from 20 runs with $R = 58.9$ and 88.4, and 8 runs for $R = 147$.
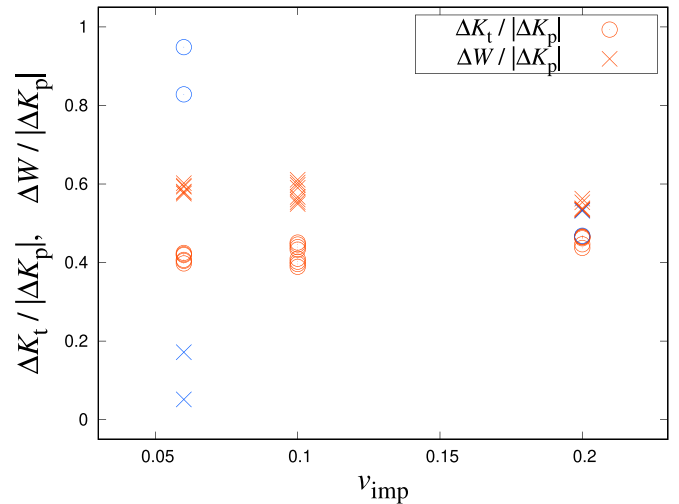

FIG. 10. The energy conversion ΔK_t and ΔW as a function of v_{imp}. The circles and crosses represent ΔK_t and ΔW, respectively. Red represents bouncing results, and blue represents the sticking cases.
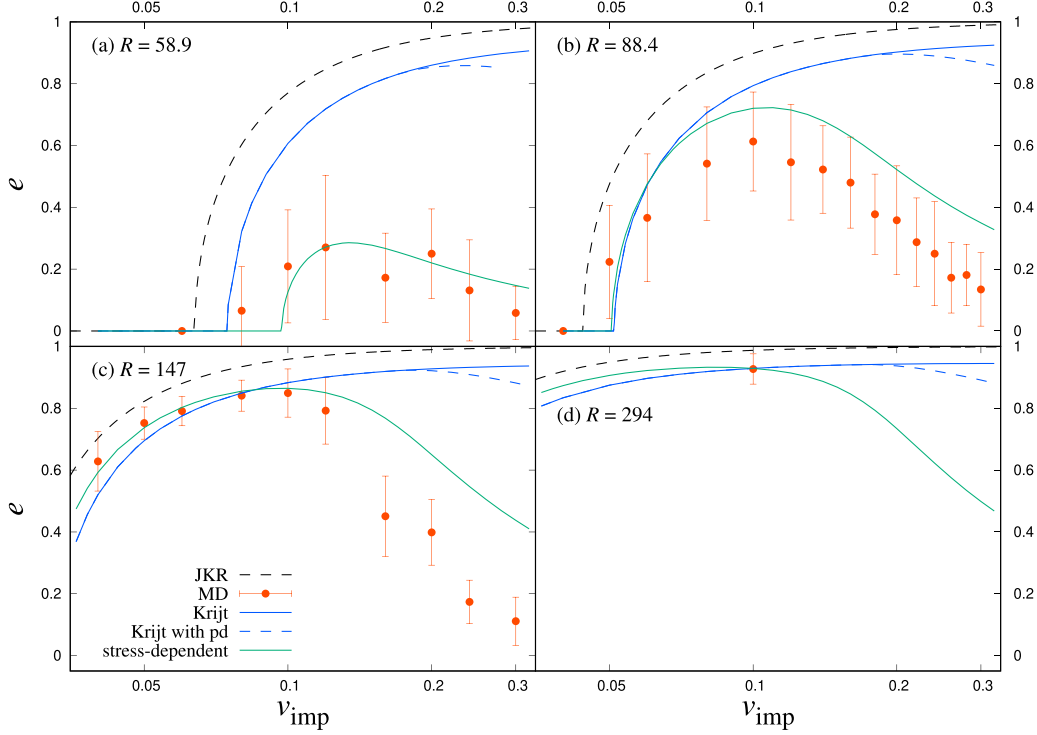
FIG. 11. Coefficient of restitution for the new model with $T_{\mathrm{vis},0}(R) \simeq 0.031(R/147)$, $B \simeq 6.4$, and $\zeta = 4.0$ as a function of v_{imp} compared to the MD simulation results and the Krijt model. The red points with error bars represent the MD results, solid blue curves represent the Krijt model, and solid green curves represent the stress-dependent dissipation model. The dashed blue curves show the Krijt model with plastic deformation (pd) for $Y = 0.12E^*$.

A. Stress-dependent dissipation model

The dissipative force of the Krijt model is in qualitative agreement with the ratio of $|F_{\mathrm{loading}} - F_{\mathrm{unloading}}|/F_c$ obtained by the MD simulations, as discussed in Sec. IV A 2. However, for the coefficient of restitution e, the MD simulation results do not agree with the Krijt model. Therefore, we discuss what the Krijt model lacks and modify the model to reproduce e.

The large energy dissipation that occurs in high-velocity collisions may be due to the high stresses in such collisions. Using Eqs. (4) and (15), we find the pressures at maximum compression to be $p_{c,\mathrm{H}} \simeq 0.194E^*$ and $0.255E^*$ for $v_{\mathrm{imp}} = 0.10$ and 0.20, respectively, in the case with $R = 147$. The maximum pressures predicted by the JKR theory are $p_{c,\mathrm{J}} = 0.211E^*$ and $0.265E^*$ for $v_{\mathrm{imp}} = 0.10$ and 0.20 for $R = 147$. Because Young's modulus E is about twice as large as E^*, the induced pressures are $\geqslant 0.1E$. Such high pressures can cause plastic deformation and, thus, strong energy dissipation. This estimate agrees with the strong energy dissipation observed in our MD simulation for high-velocity collisions. However, for small particles, the pressure p_c is not small even at the stationary contact with $\delta = \delta_0$. In fact, for $R = 58.9$ and $\delta = \delta_0$, the pressure p_c is obtained as $\sim 0.16E^*$ from Eq. (9). The JKR theory predicts $p_{c,\mathrm{J}} \simeq 0.282E^*$ for $v_{\mathrm{imp}} = 0.1$ and $R = 29.6$. Thus, for small particles with $R \leqslant 58.9$, the induced pressure can cause plastic deformation even in low-velocity collisions. This is consistent with the small values of COR shown in Fig. 8(a).

We, therefore, propose a new, stress-dependent dissipation model to reproduce the strong energy dissipation that occurs under high stress in particle collisions. In this model, we adopt the same formula for the dissipation force as in the Krijt model [Eq. (12)], although the relaxation time T_{vis} now depends on the pressure at the center of the contact area, p_c as

$$T_{\mathrm{vis}}(p_c) = \begin{cases} T_{\mathrm{vis},0}(R) \exp\left[\left(B\frac{p_c}{E^*}\right)^\zeta\right] & (p_c > 0), \\ T_{\mathrm{vis},0}(R) & (p_c < 0), \end{cases} \quad (17)$$

where $T_{\mathrm{vis},0}(R)$ and B are coefficients and ζ is a power-law-index. The pressure p_c at the center of the contact area is given by Eq. (9). The relaxation time is linear in the particle radius:

$$T_{\mathrm{vis},0}(R) = CR, \quad (18)$$

where C is a coefficient. We adopt the exponential form of T_{vis} on p_c to express the strong energy dissipation dependent on the stress. Using Eq. (17), we solve Eqs. (B2) and (10) to investigate the evolution of the contact radius and the relative motion of two particles. Then, we search for optimal values of B, C, and ζ in the range of $6.0 < B < 6.4$, $2 \times 10^{-4} < C < 5 \times 10^{-4}$ and $1 < \zeta < 5$ to fit our model to the MD simulation results.

Figure 11 shows the fitting results obtained with $B \simeq 6.2$ and $\zeta = 4.0$. Since $T_{\mathrm{vis},0} \simeq 0.031$ for $R = 147$, we obtain $C \simeq 2.1 \times 10^{-4}$. The relaxation time $T_{\mathrm{vis}}(p_c)$ is almost the same as that in the Krijt model. This new model is consistent with the MD simulation results well for $R = 58.9$ and 294. The new model also reproduces the MD simulation results in the range $v_{\mathrm{imp}} \lesssim 0.2$ for $R = 88.4$ and $v_{\mathrm{imp}} \lesssim 0.12$ for $R = 147$. Compared with the Krijt model, the new model better reproduces the MD simulation results for $R = 58.9$ and the COR peak for $R = 88.4$ and 147 for low impact velocities.
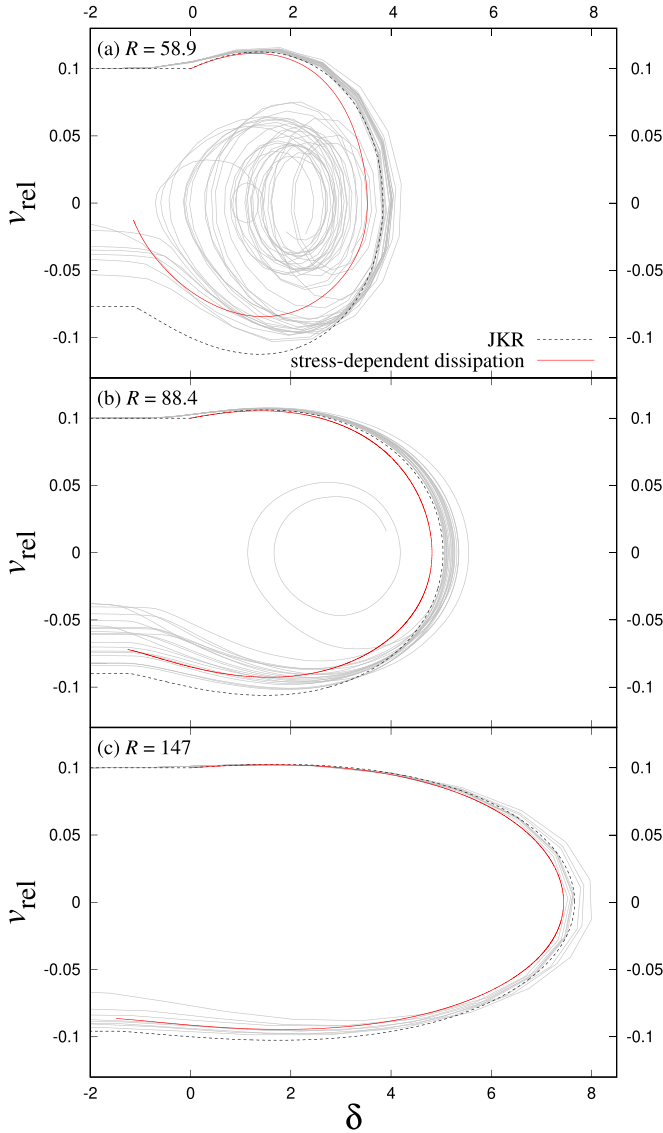
FIG. 12. Relation between δ and v_{rel} for $v_{\text{imp}} = 0.1$ and $R = 58.9$, 88.4, and 147. The black dotted curves represent the JKR theory, the gray curves represent each MD simulation result, and the red curves represent the new model. The mutual approach in the new model is smaller than in the MD simulation results.

These fitted values are expected to depend on the potential. For example, in the case of silica, the pressure at which deformation occurs is expected to be greater than for LJ atoms, and then B is expected to be smaller than that for LJ atoms. At high impact velocities, there appear to be some discrepancies between the model and the MD simulations. To achieve a more accurate reproduction at high-velocity collisions, it may be necessary to handle plastic deformation in a more precise way.

We also examine the trajectories of particles in the δ-v_{rel} phase plane to check whether the new model can reproduce the contact model by comparing the MD results. Figure 12 shows the δ-v_{rel} relation with $v_{\text{imp}} = 0.10$. We find that δ in the new model is smaller than those in either the JKR theory or the MD simulation results. Although the new model reproduces the motion of large particles well, the displacement of δ cannot

be reproduced perfectly. At $R = 58.9$ in Fig. 12, the difference of δ between the MD simulations and the new model at maximum compression is about 0.4, which may indicate plastic deformation.

B. Simple dissipation model

The Krijt and the new models described above are too complex to apply in powder simulations. We, therefore, propose a simple power-law dissipation model in which the dissipation force is given by

$$F_{\text{dis}} = \text{sgn}(v_{\text{rel}})DE^*|v_{\text{rel}}|^\alpha a^\beta, \qquad (19)$$

where D is a coefficient and α and β are power-law-indices. We include the factor $\text{sgn}(v_{\text{rel}})$ because the dissipation force and relative velocity point in opposite directions. We searched for optimal values of D, α, and β to fit the MD simulation results by solving the equation of motion:

$$m^* \frac{d^2\delta}{dt^2} = -(F_{\text{J}} + F_{\text{dis}}). \qquad (20)$$

In this model, we do not consider the time evolution of the contact radius but instead use the contact radius based on Eq. (5).

Figure 13 shows the COR for this simple model with $D = 118$, $\alpha = 3.0$ and $\beta = 1.5$. This model reproduces the MD simulation results for $v_{\text{imp}} \lesssim 0.12$. Small α and large β result in weak dissipation. We find that the appropriate values are $2.0 < \alpha < 3.0$ and $1.0 < \beta < 1.5$. Because we simply add the dissipative force to the JKR force, it is easy to use this model for powder simulations with low-velocity collisions.

VI. SUMMARY

In the present work, we have studied head-on collisions between two equal-mass particles by using molecular dynamics (MD) simulations with the Lennard-Jones (LJ) potential as the intermolecular potential. We have investigated the normal interparticle force between the macroscopic particles and the coefficient of restitution (COR) e, and we have constructed a new contact model that includes energy dissipation to reproduce the simulation results. Our main findings are summarized as follows:

(1) In the unloading phase of collisions between two particles, the interparticle force deviates from that of the JKR theory, whereas in the loading phase, it agrees with the JKR theory (Figs. 2 and 3). The difference in the force between the loading and unloading phases represents the hysteresis in the particle interaction, which dissipates the kinetic energy of the motion of each particle's center of mass. The contact radius also has hysteresis; a of the MD simulations is smaller than that of the JKR theory in the loading phase and larger in the unloading phase. The hysteresis in the force is greater for smaller particle sizes or higher collision velocities. In particular, for high-velocity collisions with $v_{\text{imp}} \gtrsim 0.2$, plastic deformation of the particle is observed (Figs. 4 and 5). The plastic deformation for $v_{\text{imp}} \gtrsim 0.2$ can be explained by the yield strength estimated by the previous studies.

(2) Energy dissipation in a collision reduces e. The CORs obtained in our MD simulations are smaller than those of
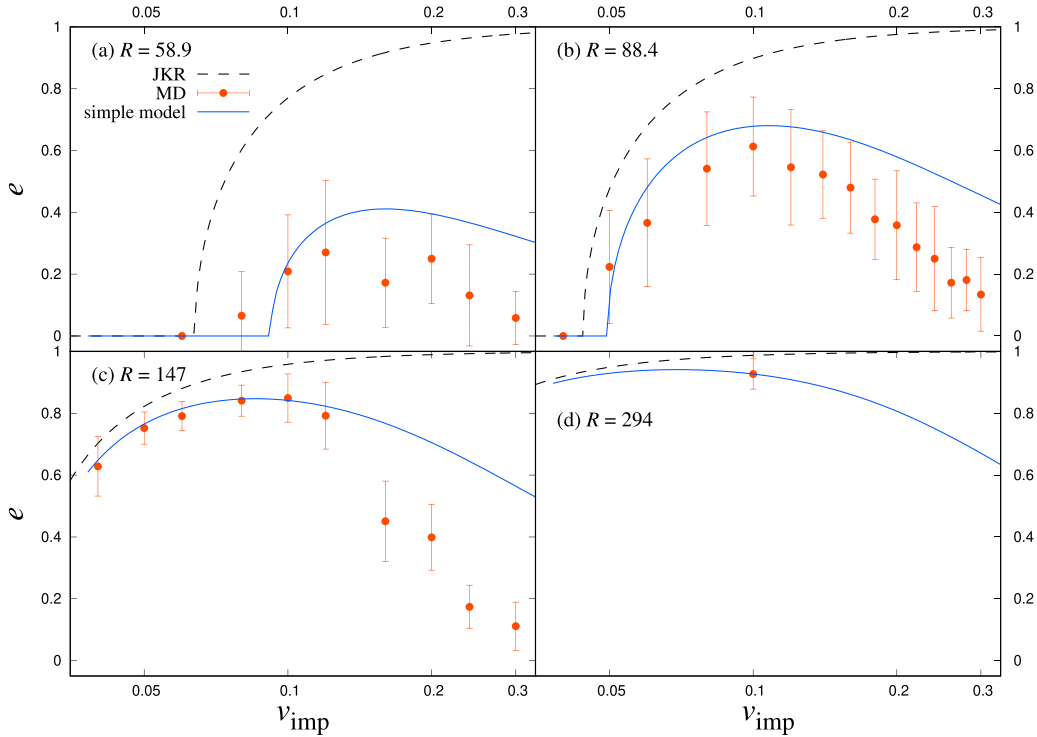
FIG. 13. Same as described in the caption of Fig. 11 but for the simple model with ($F_{\rm dis} \propto D|v_{\rm rel}|^3 a^{3/2}$).

the JKR theory, which is natural because energy dissipation occurs at any time during contact in the MD simulations. The Krijt model includes such hysteresis in the force to accurately describe the energy dissipation. For high-velocity collisions ($v_{\rm imp} > 0.1$), our MD simulations show much higher energy dissipation than that predicted by the Krijt model, although the Krijt model reproduces our simulations well for low-velocity collisions ($v_{\rm imp} < 0.1$) in Fig. 8. In contrast, the strong energy dissipation in the MD simulations for $v_{\rm imp} > 0.1$ cannot be explained even by the Krijt model with plastic deformation using the yield strength obtained by the previous MD simulations of collisions between nonadhesive particles. Collisions of adhesive particles produce additional dissipation rather than nonadhesive particles.

(3) To reproduce the strong energy dissipation observed in our MD simulations for high-velocity collisions, we have proposed a new, stress-dependent dissipation model in which the relaxation time, $T_{\rm vis}$, increases rapidly with the pressure at the center of the contact surface, $p_{\rm c}$, for $p_{\rm c} > 0.1E^*$ [Eq. (17)]. We found that the stress-dependent dissipation model successfully reproduces the CORs in our MD simulations well for $v_{\rm imp} < 0.2$. We have also proposed another simple dissipation model [Eq. (19)] that can reproduce the CORs of our MD simulations for $v_{\rm imp} < 0.2$ and which is expected to be useful for powder simulations.

The proposed new models successfully reproduce the MD results for $v_{\rm imp} < 0.2$, although the energy dissipation is insufficient for higher impact velocities. This is due to particle deformation at high impact velocities, which leads to significantly small values of the COR. Neither the Krijt model nor the proposed models include this effect. Thus, we cannot reproduce the COR of our MD simulations at high impact velocities. Both the new stress-dependent model and the Krijt

model solve for the evolution of the contact radius independently, although the dissipation due to delay of a is negligibly small in these models. We, therefore, used the same relaxation time $T_{\rm vis}$ in the dissipation force and contact radius evolution. If $T_{\rm vis}$ in Eq. (B2) is much larger than that of dissipation force, then the delay of a is more significant and can be effective in decreasing COR. This is one of the possibilities to explain our MD simulations. We thus need to understand better the property of $T_{\rm vis}$.

We also need to consider the effects of different particle properties. In this study, we used particles with an ideal FCC structure. However, we should also investigate the effects of structures such as body-centered cubic (BCC) or amorphous structures and their dependence on the filling factors of the macroscopic particles. The particle temperature also affects the collision results, and we should explore this as well in a future paper. We should also simulate particle collisions with more realistic molecules, such as water, to understand dust growth in planet-forming regions. These subjects are all planned for future work.
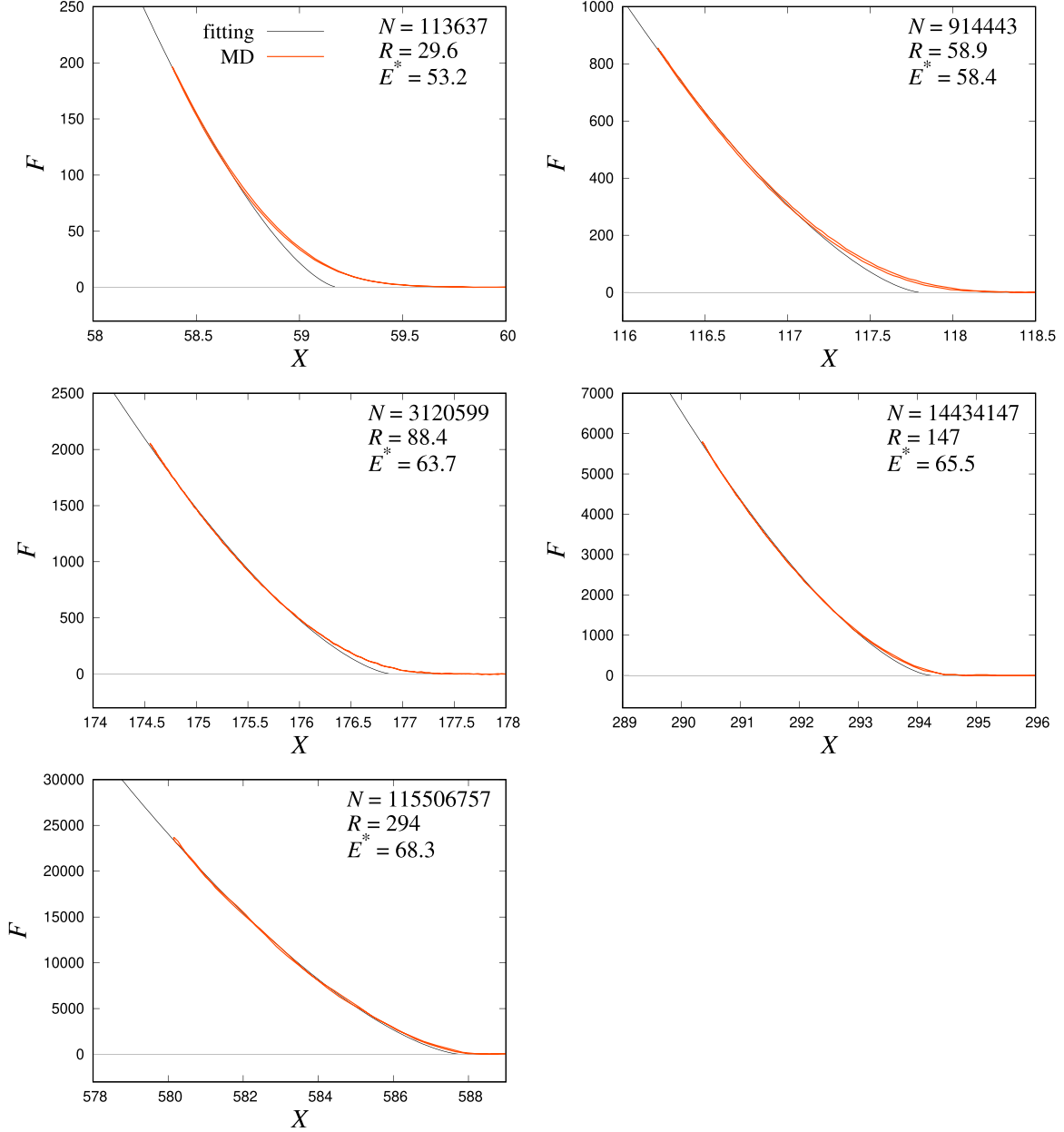
FIG. 14. The force acts on the particles. The red lines are the MD results, and the black lines are the fitting results.

APPENDIX A: DETERMINATION OF E^* AND R

We used MD simulations to determine the particle radius R and the reduced Young's modulus E^*. We prepared five particles by hollowing out atoms so that $R = 29.4, 58.8, 88.2, 147$, and 294. We also remove the attractive term $-(r/\sigma)^{-6}$ from the molecular potential between atoms belonging to different particles. The modified LJ potential then becomes

$$u_{\text{LJ,mod}}(r_{ij}) = 4\epsilon\left[\left(\frac{r_{ij}}{\sigma}\right)^{-12} - \delta_{k\ell}\left(\frac{r_{ij}}{\sigma}\right)^{-6}\right], \qquad \text{(A1)}$$

where $\delta_{k\ell}$ is the Kronecker delta, and k and ℓ represent the macroscopic particles to which the ith and jth atoms belong, respectively. In this case, the force between particles corresponds to a Hertzian contact. We calculate the force between the particles and fit the parameters R and E^* using Eq. (2).

When we fit the parameters, we ignore the data for small F since a small force works due to the intermolecular force existing even if the two particles are not in contact. Figure 14 shows the forces and fitting lines as a function of X, and Table II summarizes the fitting results. The fitting results are slightly larger than the initially prepared radii, with a difference of less than 1. Here, we simulated only one run for each radius with the same orientation as that shown in Fig. 3. Note that the fitting results may change slightly depending on the orientations.

APPENDIX B: MODEL OF CRACK PROPAGATION

Here, we summarize the crack–propagation model used in the Krijt model. The apparent surface energy is expressed

as [22]

$$G_{\text{eff}} = \frac{E^*}{4\pi a R^{*2}}(a^2 - \delta R^*)^2. \tag{B1}$$

If δ and a have the relationship shown in Eq. (5), which is satisfied by the JKR theory, then $G_{\text{eff}} = \gamma$. Because of viscoelasticity, however, the evolution of the contact area differs slightly from that of the JKR theory (e.g., Refs. [22,24]). The crack speed $\dot{a}$ can be written as [23,54]

$$\frac{\sigma_0^2 T_{\text{vis}}}{2E^*\gamma}\dot{a} = \begin{cases} 0.15\left[\beta \ln\left(\frac{0.98}{1-\beta}\right)\right]^{-1}, & (\beta \leqslant 0.29), \\ (0.1035x + 0.3421)x^{1.1160}, & (0.29 < \beta < 1, \text{ where } x = 1/\beta - 1), \\ -(0.2112x + 0.3939)x^{1.1403}, & (1 < \beta < 3.7, \text{ where } x = \beta - 1), \\ -0.24\beta\left[\ln\left(\frac{0.98}{1-1/\beta}\right)\right]^{-1}, & (3.7 \leqslant \beta), \end{cases} \tag{B2}$$

where $\beta = G_{\text{eff}}/\gamma$ and $\sigma_0 \simeq \gamma/$(spacing between atoms). We also assume the initial condition given in Appendix B of Krijt *et al.* [22].

APPENDIX C: SURFACE ENERGY

We derive the surface energy in our MD simulations using the potential energy of a spherical particle with an FCC structure of the atoms. The surface energy of a spherical particle is given by

$$\gamma = -\frac{Ne_1 - U}{4\pi R^2}, \tag{C1}$$

where N is the number of atoms in the system, and e_1 is the potential energy per atom in the FCC solid. The total potential energy of the particle, U, is obtained from our MD simulation. The energy e_1 is the value when the atoms extend to infinity, meaning there is no surface or boundary.

The energy e_1 is obtained as follows. If the LJ potential has no cutoff, then the potential energy per atom in the FCC solid, e_1, is given by [55]

$$e_1 = \frac{1}{2} \times 4\epsilon\left[\sum_j \left(p_j\frac{D}{\sigma}\right)^{-12} - \sum_j \left(p_j\frac{D}{\sigma}\right)^{-6}\right]$$
$$= 2\epsilon[a(D/\sigma)^{-12} - b(D/\sigma)^{-6}], \tag{C2}$$

where D is the nearest-neighbor distance and p_jD is the distance between a reference atom and any other atom j. For the FCC structure, the coefficients a and b are given by

$$a = \sum_j p_j^{-12} = 12.13, \quad b = \sum_j p_j^{-6} = 14.45. \tag{C3}$$

However, in this study, we set the cutoff $r_{\text{cut}} = 5.0\sigma$, so we need to include the effects of the cutoff in determining e_1.

We can neglect the cutoff effect on the coefficient a due to the rapid decreases of p_j^{-12}. There are two cutoff effects on the coefficient b. One is to set the potential to be zero at $r(= p_jD) = r_{\text{cut}}$ by replacing p_j^{-6} with $p_j^{-6} - (r_{\text{cut}}/D)^{-6}$. The resulting correction Δb_1 is given by

$$\Delta b_1 = -\left(\frac{r_{\text{cut}}}{D}\right)^{-6}\frac{4\pi}{3}\frac{r_{\text{cut}}^3}{V_1} = -\frac{4\sqrt{2}\pi}{3}\left(\frac{r_{\text{cut}}}{D}\right)^{-3}, \tag{C4}$$

where $V_1 = D^3/\sqrt{2}$ is the volume per atom in the FCC structure. The other cutoff effect on b is neglecting terms with $r > r_{\text{cut}}$. We find that the correction due to the neglect, Δb_2, equals Δb_1. Thus, including these corrections, we obtain e_1 as

$$e_1 = 2\epsilon\left[12.13\left(\frac{D}{\sigma}\right)^{-12} - \left\{14.45 - \frac{8\sqrt{2}\pi}{3}\left(\frac{r_{\text{cut}}}{D}\right)^{-3}\right\}\left(\frac{D}{\sigma}\right)^{-6}\right]. \tag{C5}$$

The nearest-neighbor distance D is determined by the equilibrium condition $de_1/dD = 0$. From the equilibrium condition with Eq. (C5), we obtain $D \simeq 1.091\sigma$ and $e_1 \simeq -8.464\epsilon$. The obtained D agrees with that of the spherical particles in our MD simulations.

The potential U is obtained from the MD simulation. We obtain $U = -9.96 \times 10^5, -7.88 \times 10^6, -2.61 \times 10^7, -1.22 \times 10^8$ for $R = 29.6, 58.9, 88.4,$ and 147, respectively, in the LJ units. Finally, we get $\gamma = 3.18, 3.18, 3.15, 3.06$, respectively. Thus, We take $\gamma = 3.17$ as the nominal value in this paper. This value agrees with that of the previous work $\gamma = 3.18$ [19].

[1] G. Reynolds, J. Fu, Y. Cheong, M. Hounslow, and A. Salman, Chem. Eng. Sci. **60**, 3969 (2005).

[2] M. Jutzi, W. Benz, and P. Michel, Icarus **198**, 242 (2008).

[3] B. Mishra and C. Thornton, Int. J. Miner. Process. **61**, 225 (2001).

[4] D. Hestroffer, P. Sánchez, L. Staron, A. C. Bagatin, S. Eggl, W. Losert, N. Murdoch, E. Opsomer, F. Radjai, D. C. Richardson, M. Salazar, D. J. Scheeres, S. Schwartz, N. Taberlet, and H. Yano, Astron. Astrophys. Rev. **27**, 6 (2019).

[5] T. Suyama, K. Wada, and H. Tanaka, Astrophys. J. **684**, 1310 (2008).

[6] K. Wada, H. Tanaka, S. Okuzumi, H. Kobayashi, T. Suyama, H. Kimura, and T. Yamamoto, Astron. Astrophys. **559**, A62 (2013).

[7] Y. Hasegawa, T. K. Suzuki, H. Tanaka, H. Kobayashi, and K. Wada, Astrophys. J. **944**, 38 (2023).

[8] Y. Hasegawa, T. K. Suzuki, H. Tanaka, H. Kobayashi, and K. Wada, Astrophys. J. **915**, 22 (2021).

[9] M. Tatsuuma, A. Kataoka, and H. Tanaka, Astrophys. J. **874**, 159 (2019).

[10] K. Wada, H. Tanaka, T. Suyama, H. Kimura, and T. Yamamoto, Astrophys. J. **677**, 1296 (2008).

[11] K. L. Johnson, K. Kendall, and A. D. Roberts, Proc. R. Soc. Lond. A **324**, 301 (1971).

[12] C. Dominik and A. G. G. M. Tielens, Philos. Mag. Part A **72**, 783 (1995).

[13] C. Dominik and A. G. G. M. Tielens, Philos. Mag. Part A **73**, 1279 (1996).

[14] C. Dominik and A. G. G. M. Tielens, Astrophys. J. **480**, 647 (1997).

[15] K. L. Johnson, *Contact Mechanics* (Cambridge University Press, Cambridge, UK, 1987).

[16] B. V. Derjaguin, V. M. Muller, and Y. P. Toporov, J. Colloid Interface Sci. **53**, 314 (1975).

[17] D. S. Dugdale, J. Mech. Phys. Solids **8**, 100 (1960).

[18] D. Maugis, J. Colloid Interface Sci. **150**, 243 (1992).

[19] H. Tanaka, K. Wada, T. Suyama, and S. Okuzumi, Prog. Theor. Phys. Suppl. **195**, 101 (2012).

[20] Y. Takato, S. Sen, and J. B. Lechman, Phys. Rev. E **89**, 033308 (2014).

[21] Y. Takato, M. E. Benson, and S. Sen, Phys. Rev. E **92**, 032403 (2015).

[22] S. Krijt, C. Güttler, D. Heißelmann, C. Dominik, and A. G. G. M. Tielens, J. Phys. D: Appl. Phys. **46**, 435303 (2013).

[23] J. A. Greenwood, J. Phys. D: Appl. Phys. **37**, 2557 (2004).

[24] N. V. Brilliantov, N. Albers, F. Spahn, and T. Pöschel, Phys. Rev. E **76**, 051302 (2007).

[25] O. V. Kim and P. F. Dunn, J. Aerosol Sci. **39**, 373 (2008).

[26] S. Wall, W. John, H.-C. Wang, and S. L. Goren, Aerosol Sci. Technol. **12**, 926 (1990).

[27] C. Anders and H. M. Urbassek, Astron. Astrophys. **647**, L13 (2021).

[28] M. L. Nietiadi, F. Valencia, R. I. Gonzalez, E. M. Bringa, and H. M. Urbassek, Astron. Astrophys. **641**, A159 (2020).

[29] M. L. Nietiadi, Y. Rosandi, and H. M. Urbassek, Nanoscale Res. Lett. **15**, 67 (2020).

[30] Y. Takato, M. E. Benson, and S. Sen, Proc. R. Soc. Lond. A **474**, 20170723 (2018).

[31] E. N. Millán, D. R. Tramontina, H. M. Urbassek, and E. M. Bringa, Phys. Rev. E **93**, 063004 (2016).

[32] M. L. Nietiadi, P. Umstätter, I. Alabd Alhafez, Y. Rosandi, E. M. Bringa, and H. M. Urbassek, Geophys. Res. Lett. **44**, 10,822 (2017).

[33] M. L. Nietiadi, Y. Rosandi, and H. M. Urbassek, Icarus **352**, 113996 (2020).

[34] M. L. Nietiadi, P. Umstätter, T. Tjong, Y. Rosandi, E. N. Millán, E. M. Bringa, and H. M. Urbassek, Phys. Chem. Chem. Phys. (Incorporating Faraday Trans.) **19**, 16555 (2017).

[35] M. L. Nietiadi, E. N. Millán, E. M. Bringa, and H. M. Urbassek, Phys. Rev. E **99**, 032904 (2019).

[36] P. Umstätter and H. M. Urbassek, Sci. Rep. **11**, 14591 (2021).

[37] A. Awasthi, S. C. Hendy, P. Zoontjens, S. A. Brown, and F. Natali, Phys. Rev. B **76**, 115437 (2007).

[38] Note that γ in this paper is equal to γ_L and twice γ of Krijt *et al.* [22].

[39] K. Wada, H. Tanaka, T. Suyama, H. Kimura, and T. Yamamoto, Astrophys. J. **661**, 320 (2007).

[40] N. V. Brilliantov, F. Spahn, J.-M. Hertzsch, and T. Pöschel, Phys. Rev. E **53**, 5382 (1996).

[41] V. M. Muller, V. S. Yushchenko, and B. V. Derjaguin, J. Colloid Interface Sci. **77**, 91 (1980).

[42] S. Arakawa and S. Krijt, Astrophys. J. **910**, 130 (2021).

[43] A. A. Griffith, Philos. Trans. R. Soc. Lond. A **221**, 163 (1921).

[44] K. Wahl, S. Asif, J. Greenwood, and K. Johnson, J. Colloid Interface Sci. **296**, 178 (2006).

[45] C. Thornton and Z. Ning, Powder Technol. **99**, 154 (1998).

[46] A. P. Thompson, H. M. Aktulga, R. Berger, D. S. Bolintineanu, W. M. Brown, P. S. Crozier, P. J. in 't Veld, A. Kohlmeyer, S. G. Moore, T. D. Nguyen, R. Shan, M. J. Stevens, J. Tranchida, C. Trott, and S. J. Plimpton, Comput. Phys. Commun. **271**, 108171 (2022).

[47] A. Michels, H. Wijker, and H. Wijker, Physica **15**, 627 (1949).

[48] J. O. Hirschfelder, C. F. Curtiss, and R. B. Bird, *Molecular Theory of Gases and Liquids* (Wiley, New York, NY, 1967).

[49] T. H. Lu and G. M. Pound, Physica Status Solidi (a) **30**, 619 (1975).

[50] D. J. Quesnel, D. S. Rimai, and L. P. DeMejo, Phys. Rev. B **48**, 6795 (1993).

[51] A. Stukowski, Modelling Simul. Mater. Sci. Eng. **18**, 015012 (2010).

[52] N. J. Petch, J. Iron Steel Inst. **174**, 25 (1953).

[53] https://www.enago.jp/.

[54] J. A. Greenwood and K. L. Johnson, J. Colloid Interface Sci. **296**, 284 (2006).

[55] C. Kittel, *Introduction to Solid State Physics*, 5th ed. (Wiley, New York, NY, 1976).